INTERNATIONAL JOURNAL OF
COASTAL & OFFSHORE ENGINEERING
IJCOE Vol.3/No. 1/Spring 2018 (67-77)

Available online at: http://ijcoe.org/browse.php?a_code=A-10-215-1&sid=1&slc_lang=en

Numerical Simulation of the Wind-Induced Current in the Caspian Sea

Jalal Mofidi [1], Akbar Rashidi Ebrahim Hesari [2*]

[1] *Ph.D. Student, Department of Marine Physics, Hormozgan University, Iran; jalal.mofidi@yahoo.com*
[2*] *Assistant Prof., Department of Marine Physics, Tarbiat Modares University, Iran; akbar.rashidi@moares.ac.ir*

ARTICLE INFO

Article History:
Received: 14 May 2018
Accepted: 13 Jun. 2018

Keywords:
The Caspian Sea
primitive equation
finite difference
wind-induced currents

ABSTRACT

A three-dimensional primitive equation model has been developed to study wind-driven currents in the Caspian Sea (CS). The equations were solved in the spherical coordinate system with a vertical array of pressure-sigma using a finite difference Method on a staggered modified Arakawa c grid. Simulations showed that there is an anticyclonic eddy over the deep water of South Caspian Basin (SCB), which extended from surface to subsurface and persist throughout the year. The model successfully produced the coastal current along the eastern coast of the Middle Caspian Basin (MCB) with a prevailing southward component, resulting in upwelling on these coasts to compensate the surface drift. The results indicate that the bottom topography has a key role in steering currents and generated a divergence in the surface Ekman layer which balanced by convergence in the frictional bottom Ekman layer in deepest areas of the CS.

1. Introduction

The CS is the largest surrounded body of water on the Earth that constituting 44% of the global volume of lakes water and area of about 379,000 km^2. Abundant resources of oil and natural gas were found around and underwater of the CS caused the surrounding countries have started developing onshore and offshore exploitation facilities. These facilities developments have released a vast amount of pollutants into the water. These pollutants have accumulated into the water or sediment since there are no runoffs from the CS. This amount of pollutants might cause a collective death of living organisms such as a large die-off of seals during the spring of 2000[1]. Many of previous studies have been involved in monitoring projects for environmental impact assessment of pollutants transport in the CS and have been focused on biological and chemical environmental impacts, while water circulation has an important role in advection and diffusion of pollutants, it has been little measured and compared with other semi-enclosed and enclosed seas of the world, little is known of the CS variability [2]. The most urgent, still unresolved questions relating to the CS are: what is the 3-D general circulation of the sea and how is this circulation produced? The phenomenological evidence is too obscure or insufficient to give acceptable answers to these questions.

The CS has an elongated geometry that its longitudinal extent is three times larger than its latitudinal one (1000 km vs. 200-400 km), resulting in great variability of climatic conditions over the sea. There are three distinguished basins according to the geographical and topographical features: the northern shallow basin, central, and southern relatively deep basins. The North Caspian Basin (NCB) is a shallow extension with a maximum depth of 20 m. The central and the southern basins have maximum depths of 788 and 1025 m, respectively, and an underwater extension of the Apsheron peninsula with a maximum depth about 180 m separates two basins. Continental shelves areas with depth less than 100 m, mainly along the northern and eastern coasts, account for 62% of the total area of the sea [3].

The CS is enclosed sea and tidal currents are negligible. Many previous studies on the water circulation of the CS have shown that winds are primarily responsible for controlling the circulation, and changes in other forces (precipitation, evaporation and rivers run off) did not have any significant effects [3-6]. The elongated geometry and complex bottom topography of the CS, acted upon by variable wind forcing result in spatially and temporally variable currents in this basin [4, 7].

Despite the history of current observations in the CS over more than half a century, there has been a lack of data for an adequate reconstruction of the water circulation and its seasonal variability. This is due to

the fact that most of currents measurements were short-term in time, conducted in coastal areas shallower than 100m, and characterized by a small number of observational data [6, 8, 9, and 10].

Numerical modelling is one of the powerful instruments to understand water circulation as well as measurement. Several previous numerical simulations of water circulation in the CS were done using diagnostic models [6, 10, 11, 12 and 13]. The success of these models was limited due to low spatial resolution (50 km), lack of the available hydrological data and hydrodynamics structure of them. Korotenko et al. simulated the dispersal of oil due to the currents generated by constant wind using the Princeton Ocean Model (POM) in the coastal water of the CS [14]. Kara et al. investigated the impact of the wind, rivers discharge, evaporation, precipitation and salt fluxes on the sea surface current in the CS using a Hybrid Coordinate Ocean Model (HYCOM) [15]. The seasonal variability of the water circulation, sea level, and air-sea interaction in the CS were simulated by Ibrayev et al. using development of a three-dimensional primitive equation numerical Model in z-level[4]. Gunduz and Ozsoy have been investigated the wind and buoyancy-driven seasonal circulation in the Caspian Sea by using of HYCOM [16].

In recent decades, few numerical models have been specially developed to study circulation pattern in the CS. Ibrayev [17] developed a three-dimensional primitive equation numerical model (MESH) in spherical coordinates system with vertical array Z for simulation of water circulation in the CS. A conjunctive numerical model consisting of a 2D depth average model and a 3D pseudo compressible model in the Cartesian coordinate system was developed by Zounemat Kermani and Sabbagh Yazdi to simulate wind driven current in the CS [18]. Kitazawa and Yang (2012) simulated water circulation in the CS by means of developmet of a three dimensional numerical simulation based on a hydrodynamic ocean model (MEC) in the Cartesian coordinate system [19]. Nasimi and Ghiassi (2006) also developed a three-dimensional model of water circulation of the CS in the Cartesian coordinate system [20].

With regard to three basins with complex bottom topography and vast shallow water area in the CS, using numerical models in z-level is associated with many problems such as numerical instability. In addition, there is no possibility of accurately determining the topography and variability of the free surface level. Also, the lower number of vertical layers in shallow water areas reduces the accuracy of simulation of currents variations along the vertical direction in these areas. Therefore using of Sigma coordinate system in the vertical direction caused the numerical mesh fits the free surface and bed very closely that providing a higher resolution near boundaries. In addition, the number of layers along the vertical direction in the shallow water and deep areas is the same, which makes it possible to better understand of variability of currents at different depths of water. One of the other benefits of this model is the ability to couple with atmospheric models, as a result of using pressure sigma coordinate in vertical direction.

2. Model description

2.1. The basic equations in pressure-sigma coordinate

The pressure-sigma coordinate system is applied in the vertical direction. Since the bottom pressure can vary with time and space, the normalized pressure-Sigma coordinate has therefore been adopted, which is defined as [21]:

$$\sigma = \frac{p - p_a}{p_b - p_a} \tag{1}$$

Where p is the pressure, p_a is atmospheric pressure at the sea surface and p_b is the sea bottom pressure. Sigma will always be 0 at the sea surface at any time, and 1 at the sea bottom.

The primitive equation was rewritten in the spherical pressure-Sigma coordinate system using the method introduced by Kasahara [22]. In this method, a generalized vertical coordinate σ is assumed to be related to the height z by a single-valued monotonic function. In terms of the z coordinate, σ is a function of x, y, z, and t, as follows:

$$\sigma = \sigma(x,y,z,t) \tag{2}$$

On the other hand, in terms of σ as a vertical coordinate, z becomes a dependent variable, so that

$$z = z(x,y,\sigma,t) \tag{3}$$

Any other scalar (or vector) dependent variable, say A, can be expressed in terms of either coordinate system as $A(x,y,z,t)$ or $A(x,y,\sigma,t)$. These functions become identical when either z or σ is replaced by its functional form in terms of the other, as follows:

$$A(x,y,\sigma,t) = A(x,y,z(x,y,\sigma,t),t) \tag{4}$$

When a partial derivative is taken with respect to s, where s is x, y, or t, the result can be expressed by the following equation:

$$\left(\frac{\partial A}{\partial s}\right)_\sigma = \left(\frac{\partial A}{\partial s}\right)_z + \frac{\partial A}{\partial \sigma}\frac{\partial \sigma}{\partial z}\left(\frac{\partial z}{\partial s}\right)_\sigma \tag{5}$$

Where the subscript z or σ denotes the vertical coordinate. Similarly, the vertical derivatives are related as follows:

$$\frac{\partial A}{\partial \sigma} = \frac{\partial A}{\partial z}\frac{\partial z}{\partial \sigma} \tag{6}$$

or alternatively

$$\frac{\partial A}{\partial z}=\frac{\partial A}{\partial \sigma}\frac{\partial \sigma}{\partial z} \tag{7}$$

When (7) is substituted into (6), the result can be written as:

$$\left(\frac{\partial A}{\partial s}\right)_{\sigma}=\left(\frac{\partial A}{\partial s}\right)_{z}+\frac{\partial A}{\partial \sigma}\frac{\partial \sigma}{\partial z}\left(\frac{\partial z}{\partial s}\right)_{\sigma} \tag{8}$$

The last expression can be used successively with s = x and y to form the gradient of *A* and a vector *B* to give the two-dimensional divergence with the following equations:

$$\vec{\nabla}_{\sigma}A=\vec{\nabla}_{z}A+\frac{\partial A}{\partial \sigma}\frac{\partial \sigma}{\partial z}\vec{\nabla}_{\sigma}z \tag{9}$$

$$\vec{\nabla}_{\sigma}\cdot\vec{B}=\vec{\nabla}_{z}\cdot\vec{B}+\frac{\partial \vec{B}}{\partial \sigma}\frac{\partial \sigma}{\partial z}\cdot\vec{\nabla}_{\sigma}z \tag{10}$$

When s = t in (8), the result is defined as follows:

$$\left(\frac{\partial A}{\partial t}\right)_{\sigma}=\left(\frac{\partial A}{\partial t}\right)_{z}+\frac{\partial A}{\partial \sigma}\frac{\partial \sigma}{\partial z}\left(\frac{\partial z}{\partial t}\right)_{\sigma} \tag{11}$$

By using of the (8), can be written the transformation of horizontal derivatives from Spherical coordinates to pressure-sigma coordinate by the following equations:

$$\begin{cases}\left(\dfrac{\partial A}{\partial \lambda}\right)_{r}=\left(\dfrac{\partial A}{\partial \lambda}\right)_{\sigma}+\dfrac{\rho}{p_b-p_A}\dfrac{\partial A}{\partial \sigma}\left(\dfrac{\partial \Phi}{\partial \lambda}\right)_{\sigma}\\ \left(\dfrac{\partial A}{\partial \varphi}\right)_{r}=\left(\dfrac{\partial A}{\partial \varphi}\right)_{\sigma}+\dfrac{\rho}{p_b-p_A}\dfrac{\partial A}{\partial \sigma}\left(\dfrac{\partial \Phi}{\partial \varphi}\right)_{\sigma}\\ \dfrac{\partial A}{\partial r}=-\dfrac{\rho g}{p_b-p_A}\dfrac{\partial A}{\partial \sigma}\end{cases} \tag{12}$$

Where λ is the longitude, ϕ latitude, r radius of the Earth, ρ density, g acceleration due to gravity and Φ geopotential.

By using this method the horizontal momentum equations in pressure-sigma coordinate can be expressed by the following equations:

$$\begin{aligned}&\frac{\partial u}{\partial t}+\frac{u}{r\cos\phi}\frac{\partial u}{\partial \lambda}+\frac{v}{r}\frac{\partial u}{\partial \phi}-w\frac{\rho g}{p_b-p_A}\frac{\partial u}{\partial \sigma}=\\ &\frac{uv\tan\phi}{r}-\frac{uw}{r}+fv-ew\\ &-\frac{\alpha}{r\cos\phi}\left[\frac{\partial p}{\partial \lambda}+\frac{\rho}{p_b-p_a}\frac{\partial p}{\partial \sigma}\left(\frac{\partial \Phi}{\partial \lambda}\right)\right]+F_{\lambda}\end{aligned} \tag{13}$$

$$\begin{aligned}&\frac{\partial v}{\partial t}+\frac{u}{r\cos\phi}\frac{\partial v}{\partial \lambda}+\frac{v}{r}\frac{\partial v}{\partial \phi}-w\frac{\rho g}{p_b-p_A}\frac{\partial v}{\partial \sigma}=\\ &-\frac{u^2\tan\phi}{r}-\frac{uw}{r}-fu\\ &-\alpha\frac{1}{r}\left[\frac{\partial p}{\partial \phi}+\frac{\rho}{p_b-p_A}\frac{\partial p}{\partial \sigma}\left(\frac{\partial \Phi}{\partial \phi}\right)\right]+F_{\phi}\end{aligned} \tag{14}$$

Where

$$\frac{d...}{dt}=\frac{\partial...}{\partial t}+\frac{u}{r\cos\phi}\frac{\partial...}{\partial \lambda}+\frac{v}{r}\frac{\partial...}{\partial \phi}-w\frac{\rho g}{p_b-p_A}\frac{\partial...}{\partial \sigma} \tag{15}$$

Where u and v are the zonal and meridional velocity components, w the vertical Velocity, $f=2\Omega\sin\phi$ $e=2\Omega\cos\phi$ Coriolis parameters, Ω representing the angular velocity of Earth's rotation, F_{λ} and F_{ϕ} are frictional forces per unit mass.

The hydrostatic equation is obtained from the relation:

$$\frac{\partial \Phi}{\partial \sigma}=-\frac{p_b-p_A}{\rho} \tag{16}$$

The continuity equation is:

$$\begin{aligned}&\frac{1}{p_b-p_A}\frac{D}{Dt}\left(p_b-p_A\right)+\frac{1}{r\cos\phi}\frac{\partial u}{\partial \lambda}\\ &+\frac{1}{r}\frac{\partial v}{\partial \phi}+\frac{\partial \dot{\sigma}}{\partial \sigma}=0\end{aligned} \tag{17}$$

Where $\dot{\sigma}=\dfrac{d\sigma}{dt}$ is the representative of vertical velocity and obtained by integrating the continuity equation from the surface to an arbitrary vertical depth, as follows:

$$\begin{aligned}\dot{\sigma}(\sigma)=&-\frac{\sigma}{p_b-p_A}\frac{\partial}{\partial t}\left(p_b-p_A\right)-\\ &\frac{1}{p_b-p_A}\left\{\begin{aligned}&\int_{\sigma=0}^{\sigma=\sigma}\frac{1}{r\cos\phi}\frac{\partial}{\partial \lambda}\left[\left(p_b-p_A\right)u\right]d\sigma\\ &-\int_{\sigma=0}^{\sigma=\sigma}\frac{1}{r}\frac{\partial}{\partial \phi}\left[\left(p_b-p_A\right)v\right]d\sigma\end{aligned}\right\}\end{aligned} \tag{18}$$

The state equation of seawater is [22]:

$$\rho(S,T,p)=\frac{\rho(S,T,0)}{1-p/K_T(S,T,p)} \tag{19}$$

Where S and T are the salinity and temperature of sea water, K_T is the thermal diffusivity coefficient.

The geopotential height was calculated by integrating the hydrostatic equation from sea bottom to a specific depth, and can be written as:

$$\Phi_{(i,j,\sigma)}=\Phi_{(i,j,\sigma=1)}+\frac{\left(p_b-p_a\right)\left(1-\sigma\right)}{\langle\rho\rangle} \tag{20}$$

Where $\langle\rho\rangle$ is the mean density and calculated by the following equation:

$$\langle \rho \rangle = \frac{1}{1-\sigma} \int_{\sigma=1}^{\sigma=\sigma} \rho d\sigma \tag{21}$$

The pressure was calculated by the following equation:

$$p = p_A + \sigma \left(p_b - p_A \right) \tag{22}$$

In order to apply the hydrodynamic effects in the model, the Bottom pressure tendency equation is obtained by integrating the continuity equation from the sea surface to the sea bottom by the following equation:

$$\frac{\partial p_b}{\partial t} = -\int_{\sigma=0}^{\sigma=1} \frac{1}{r \cos\phi} \frac{\partial}{\partial \lambda} \left[\left(p_b - p_A \right) u \right] d\sigma - \int_{\sigma=0}^{\sigma=1} \frac{1}{r} \frac{\partial}{\partial \phi} \left[\left(p_b - p_A \right) v \right] d\sigma + \frac{\partial p_a}{\partial t} \tag{23}$$

The terms including the velocity in the above relation are the hydrodynamic parts of pressure distribution.

The finite difference method was employed for the numerical solution of model equations. The Lax-Wendroff and Dufort-Frankel schemes were used for advection and diffusion terms respectively. The Dufort-Frankel scheme is unconditionally stable since the Courant-Friedrichs-Lewy stability condition must be satisfied for the Lax-Wendroff scheme [24]. The staggered modified Arakawa C grid was used for the spatial discretization in this model.

2.2 Boundary Condition

The No-slip condition was used at lateral boundaries that tangential and normal components of velocity were set to be zero as follows:

$$\begin{cases} u(\lambda, \varphi, \sigma, t) \cdot \mathbf{n} = 0 \\ v(\lambda, \varphi, \sigma, t) \cdot \mathbf{n} = 0 \end{cases} \tag{24}$$

$$\begin{cases} u(\lambda, \varphi, \sigma, t) \cdot \mathbf{t} = 0 \\ v(\lambda, \varphi, \sigma, t) \cdot \mathbf{t} = 0 \end{cases} \tag{25}$$

Where $\mathbf{n}$ and $\mathbf{t}$ are the normal and tangential unit vectors.

At the sea surface the corresponding boundary conditions are:

$$p = p_A \tag{26}$$

$$\left(\frac{-\mathbf{A}_\sigma g}{p_b - p_A} \frac{\partial u}{\partial \sigma}, \frac{-\mathbf{A}_\sigma g}{p_b - p_A} \frac{\partial v}{\partial \sigma} \right) = \left(\frac{\tau_{s\lambda}}{\rho}, \frac{\tau_{s\phi}}{\rho} \right) \tag{27}$$

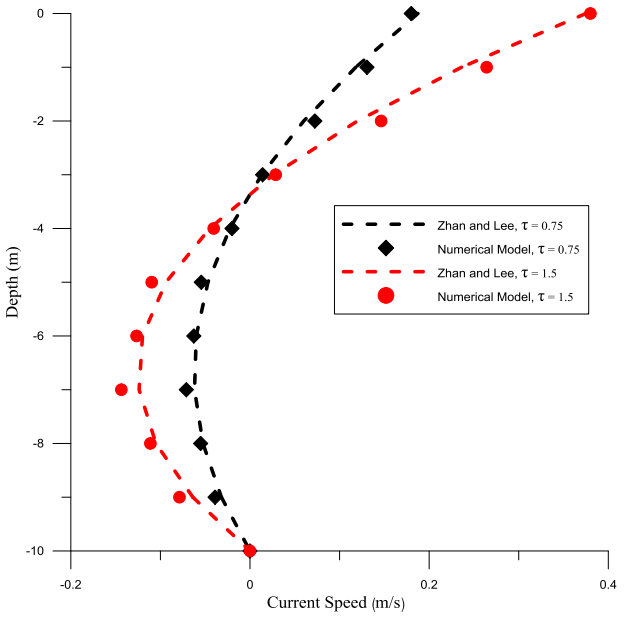

Fig.1. Comparison of numerical model predictions with analytical solution at the centre of the basin.

Where $\tau_{s\lambda}$ and $\tau_{s\phi}$ are the Sea surface frictional stresses caused by the wind in the longitude and latitude directions and can be calculated by:

$$\left(\tau_{s\lambda}, \tau_{s\phi} \right) = \left(c_D \rho_a |\mathbf{V}_{10}| u_{10}, c_D \rho_a |\mathbf{V}_{10}| v_{10} \right) \tag{28}$$

Where $\mathbf{V}_{10} = \left(u_{10}, v_{10} \right)$ is the wind velocity vector at 10 meters above the sea surface, ρ_a is air density equal 1.3 kg m^{-3}. C_D is the drag coefficient and calculated by Wu method as follows [25]:

$$c_D = \begin{cases} \left(0.8 + 0.065 |\mathbf{V}_{10}| \right) \times 10^{-3} & |\mathbf{V}_{10}| > 7.5 ms^{-1} \\ 1.2875 \times 10^{-3} & |\mathbf{V}_{10}| < 7.5 ms^{-1} \end{cases} \tag{29}$$

At the sea bottom, the boundary condition can be written as:

$$p = p_b \tag{30}$$

$$\left(\frac{-\mathbf{A}_\sigma g}{p_b - p_A} \frac{\partial u}{\partial \sigma}, \frac{-\mathbf{A}_\sigma g}{p_b - p_A} \frac{\partial v}{\partial \sigma} \right) = \left(\frac{\tau_{b\lambda}}{\rho}, \frac{\tau_{b\phi}}{\rho} \right) \tag{31}$$

Where $\tau_{b\lambda}$ and $\tau_{b\phi}$ are bottom frictional stresses in longitude and latitude directions respectively, and can be calculated by Nihoul's method as follows [26]:

$$\tau_b = -m \tau_s + D \bar{\mathbf{V}} |\bar{\mathbf{V}}| \tag{32}$$

Where τ_b is the bottom friction, $\bar{\mathbf{V}}$ is the mean flow velocity, m=0.07 and D=211×10^{-5} are two empirical coefficients.

2.3 Numerical model validation and sensitivity analyses

To prove the model accuracy and efficiency, a comparison of the model predictions with analytical solutions was performed for a standard case in a rectangular basin. This experiment was examined the vertical profile of horizontal velocity in a closed basin with a flat bed and with non-slip bottom condition.

In this test case, the Coriolis effect and the horizontal diffusion and cross (y-direction) terms were neglected, leading to a balance between the gravitational force due to the surface elevation gradient, the vertical diffusion of momentum, and the surface wind stress and the bottom friction term in the momentum equation. The analytical solution for the horizontal velocity component in a well-mixed channel with a known constant vertical eddy viscosity coefficient is calculated by method introduced by Li and Zhan as follows [27]:

$$u=\frac{\sigma(h+\eta)(3\sigma-2)}{4A_v\rho}\tau_{xz}^{s} \tag{33}$$

Where $\sigma=\frac{h+z}{h+\eta}$, u is the horizontal velocity, τ_{xz}^{s} is the surface wind stress, A_v is the vertical eddy viscosity, η is the surface elevation, *h* is the total water depth, z is the vertical coordinate which is equal to zero at the sea surface and equal to *h* at the sea bottom. In the numerical simulations, the following parameters were used;

h = 10 m, g = 9.8 m s^{-2}, ρ = 1025 kg m^{-3}, A_v = 0.01 m^2 s^{-1}; Δt = 5 s; f = 0.

The test basin was rectangular, with an area of 2 km long × 2 km wide and depth of 10 m. the simulations were performed using 21 pressure Sigma vertical layers and with a square grid by size of 100 m in both longitude and latitude directions. For this test case two steady wind conditions were applied, where the wind stress was set to τ_{xz}^{s} = 0·75 and τ_{xz}^{s} = 1.5 N m^2, respectively. The model was started with a zero velocity field and surface elevation and the simulation continued under constant wind stress. Comparisons of the model predictions with analytical solutions at the centre of the basin are shown in Fig. 1 where it can be seen that, as expected, the upper layer currents are in the wind direction whereas the lower layer currents are in the opposite direction, to maintain mass balance in the closed basin.

The Mean Absolute Percentage Error (MAPE) was used to calculate error rates. MAPE usually expresses accuracy as a percentage, and is defined by the following relation:

$$MAPE=\frac{1}{n}\sum_{i=1}^{n}\left|\frac{A_i-N_i}{A_i}\right|\times 100 \tag{34}$$

Where A_i is the analytical value and N_i is the numerical value. The comparison showed a discrepancy of approximately 10% between the numerical and analytical solution for wind stress 0.75 and about 8% for wind stress 1.5 N m^{-2}.

The Root Mean Square (RMS) Error value between prediction and analytical solution was found to be very small. The calculated RMS values for the wind stress of 0.75 and 1.5 N m^{-2} were equal to 0.007 and 0.015, respectively.

Several tests and sensitivity analysis were performed during the preparation of the model. The model was tested in a rectangular standard case study against the number of layers and cells, with and without Coriolis force, different depths, different vertical eddy viscosities, constant and variable amount of sigma. After achieving ideal conditions, the model was tested against actual bottom topography of the CS and different wind conditions. By eliminating the model's instabilities sources, the final model was used to simulation of wind induced currents in the Caspian Sea.

2.4 Model Inputs.

In the numerical simulation, the number of layers in vertical direction is equal to 21, time step is equal to 5 s, space step is equal to 0.125 degree, the number of points in longitude direction is 73 and in latitude directions is 97, salinity of sea water at the surface layer is equal to 20 ppt and sea surface temperature is equal to 25 c^o. The other model parameters in the numerical simulations were: Horizontal eddy viscosity = 10^2 m^2 s^{-1}, Vertical eddy viscosity = 10^{-2} m^2 s^{-1}, Air pressure = 101300 pa, Earth radius = 6370949 m and earth angular velocity = 7.2921 ×10^{-5} rad s^{-1}.

2.4.1 Bathymetry data

Fig. 2 shows the bottom topography of the CS. The model uses bathymetric data obtained from the General Bathymetric Chart of the Oceans (GEBCO) datasets. The minimum depth in the model is 3 m in the NCB, and a maximum depth of 1025 m occurs in the SCB. The grid resolution of the model is equal to 0.125^o in both latitude and longitude directions. The model grid area covers the entire CS from 36° to 48° N and 46° to 55° E.

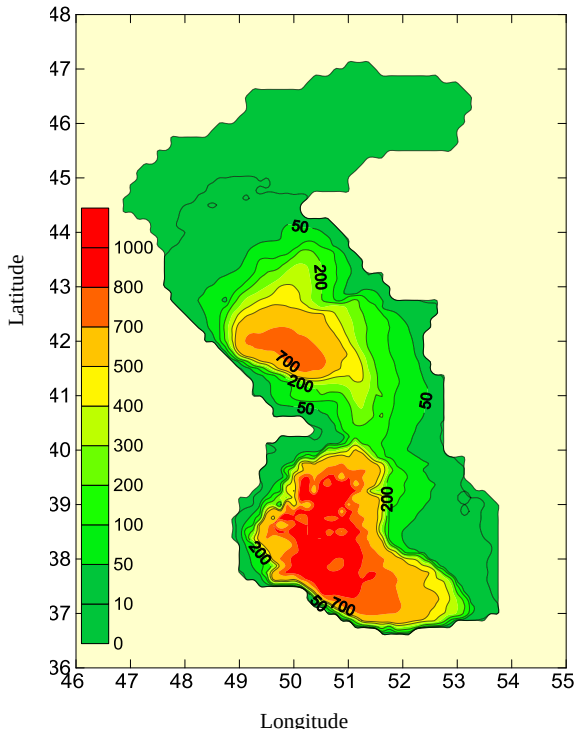

Fig.2. Bottom topography of the Caspian Sea (depths in meters).

2.4.2 Wind.

The spatiotemporally varying wind data in 10 meters height above the sea surface available from the European Centre for Medium-Range Weather Forecasts reanalysis (ECMWF ERA15) dataset for 1982, was utilized in the model. The substantial agreement is observed between these data and the climatologic winds measurements made at ships and 72 coastal meteorological stations [3]. The wind data time step is 24 hours (daily) and the data resolution is 0.125^{o} both in latitude and longitude directions. Fig. 3 shows Monthly mean wind velocity vectors computed based on the ECMWF ERA15 data set in 1982. The monthly mean wind speed is typically between 3-6 m s^{-1} during the selected year with a maximum of 5.8 m s^{-1} in June and a minimum of 3.2 m s^{-1} in December. The strongest winds occur in the SCB during February till November. In most months of the year, the north-northeast ward winds prevail in the NCB, and the southeast and southwest ward winds prevail in the MCB, Also, the south-southwest ward winds are dominated throughout the year in the SCB.

3. Result

The annual mean surface currents are computed based on the model results are shown in Fig. 4. They are generally found to be weak, with maximum values of about 5 cm s^{-1} in shallow water areas in the NCB and near the eastern coast of the SCB, as has also been noted numerically by Korotenko et al. and Ibraev et al., as well [14, 28]. Although surface currents driven by daily winds demonstrate significant variability, this is not reflected in the annual averaged circulation. According to Fig.4, an anticyclonic gyre almost entirely covered the MCB, also a sub-basin scale anticyclonic gyre is found in the SCB.

The Fig.5 shows the monthly averaged surface currents in the CS. In most month of the year, the east and northeast ward surface currents dominated in the NCB. The wind direction changes during February (Fig.3) and May (not shown), resulting change in current direction to become southeast and southwest ward respectively.

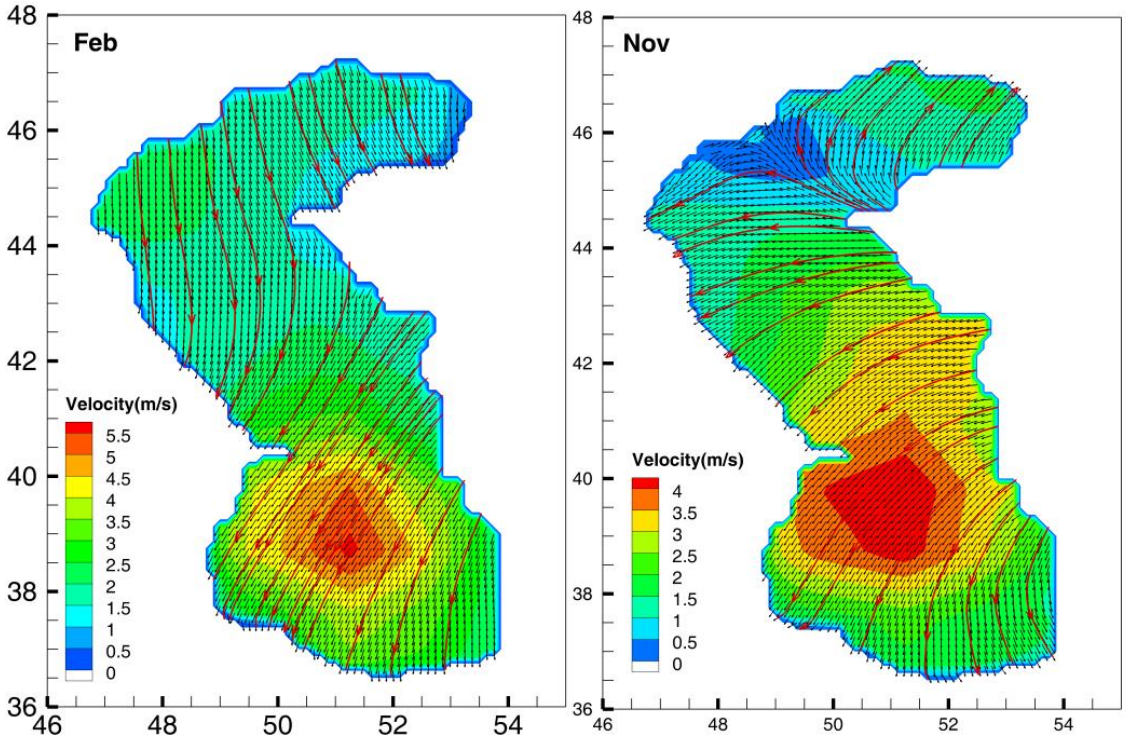

Fig.3. Monthly mean wind velocity vectors based on the ECMWF ERA15 data set.

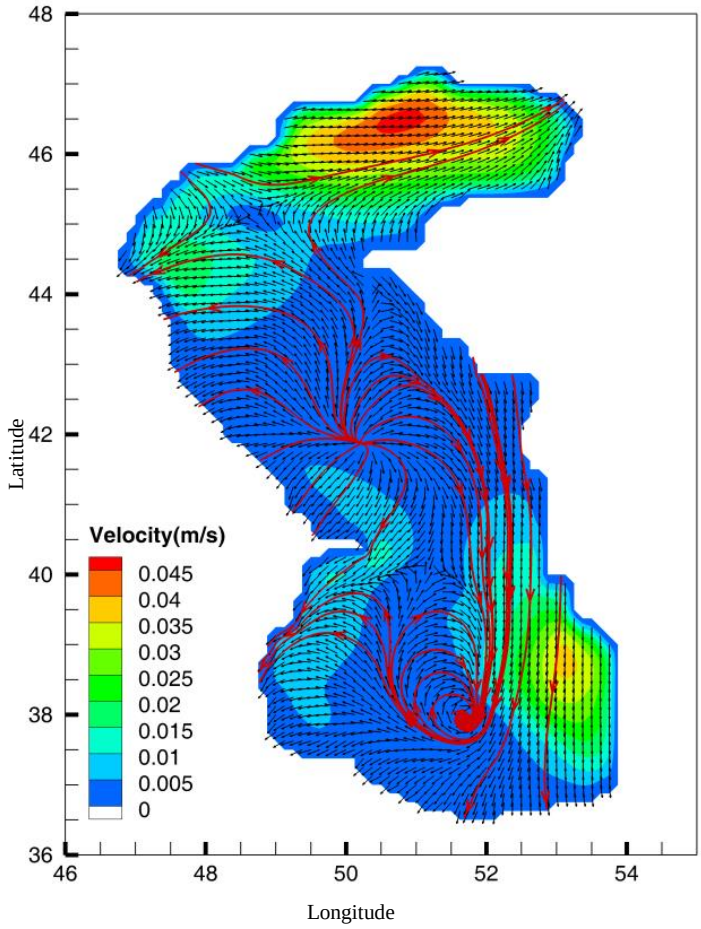

Fig.4. Annual mean surface current (m s^{-1}) in the Caspian sea

The circulation pattern in the eastern coast of the MBC can be divided into two periods (Fig.5): a) February-July when the southeast ward surface current resulting in an offshore transport of water mass and upwelling along these coasts, as has also been noted by Kosarev and Yablonskaya; Terziev et al.; Kara et al. and Ibrayev et al. [3-6]. b) August-January when the wind direction gradually changes cause a clockwise rotation in surface current to become northwest ward, resulting in onshore transport of water mass and downwelling along these coasts. This effect was also noted by Lednev and Ibrayev et al. [4, 29]. Also, there are found a divergence of surface currents over the deep water of MCB in most months of the year and an anticyclonic eddy in February which extended from surface to subsurface. An anticyclonic eddy and its adjacent currents are diverged in deeper regions of the SCB and establish a counter clockwise alongshore current near the western coasts and an eddy extended from surface to subsurface. An anticyclonic eddy and its adjacent currents are diverged in deeper regions of the SCB and establish a counter clockwise alongshore current near the western coasts and an eddy in the middle part of the basin all year round. The surface currents are very sensitive to change of wind direction and speed near the eastern coasts of the SCB due to the vast continental shelf of this area. The maximum of surface current velocities in the SCB usually take place near this coast. In most month of the year, the south and southwest ward surface currents dominated in this area, and change of wind direction to southeast ward during April to July resulting in change the direction of the surface current to become southeast ward.

The monthly averaged currents in subsurface layers in February are shown in Fig. 6. The maximum of monthly mean velocity of the surface and subsurface currents take place in the NCB in February. The depths of these areas are less than 10 m. By increase the depth the direction of southeast ward surface currents in the NCB changes to the northwest ward and the maximum of current velocity are reduced from 14.2 to 2.32 cms^{-1} on the fifth layer of sigma coordinates. The directions of currents in the next layers are in the northwest ward and the maximum of current velocity increases in the eighth layer to 5 cm s^{-1} due to the low depth of this area and changing the direction of current to compensate offshore currents at the surface. The maximum of current velocity decreases in the tenth layer to 1.78 cm s^{-1} due to the influence of bottom friction.

In the MCB, the anticyclonic eddy continues until the third layer and as the depth increases, the currents becomes to the northwest ward. The south and southeast ward along shore currents near the eastern coasts of MCB rotate clockwise by increasing the depth. They are completely in the opposite direction of surface current on the fifth layer to compensate the offshore transport of water mass on the surface layer.

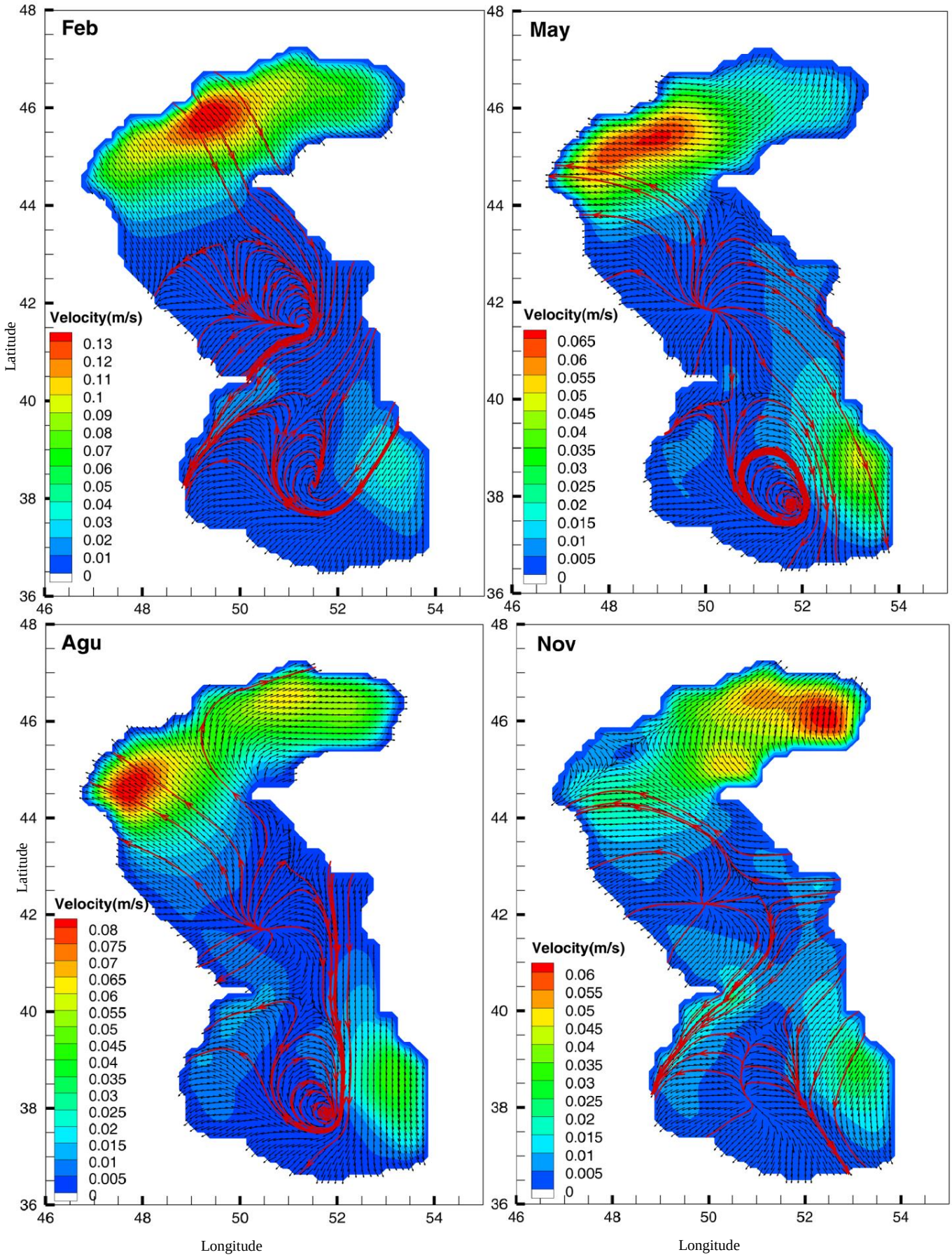

Fig.5. Monthly means surface currents (m s^{-1}) in the Caspian Sea.

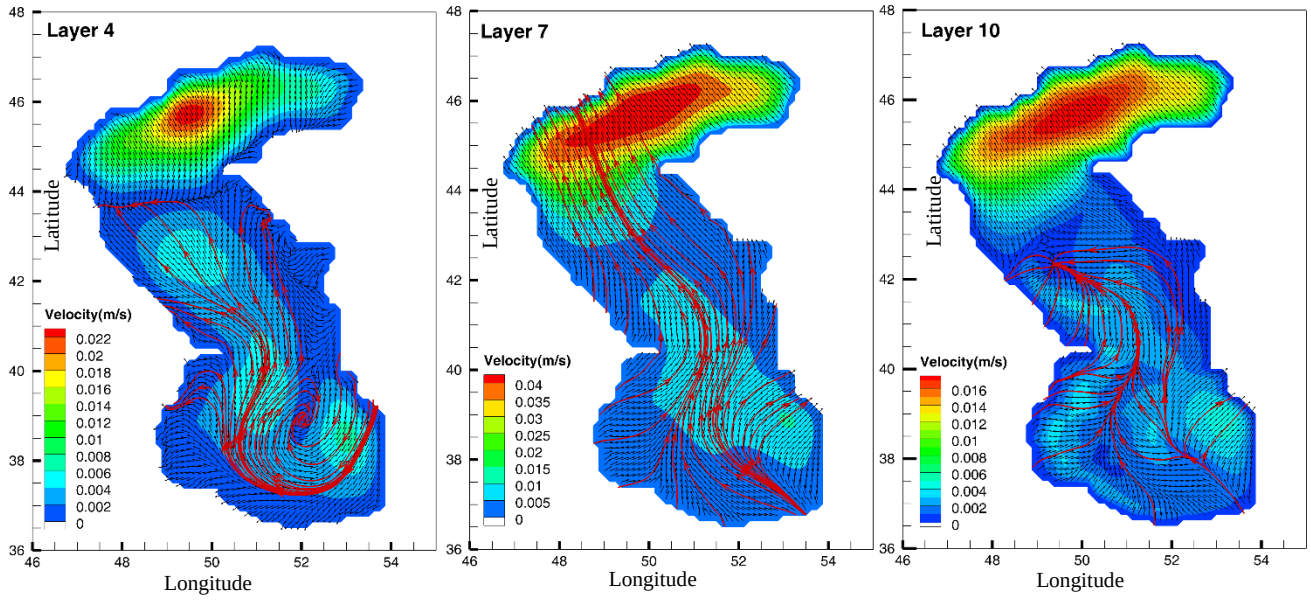

Fig.6. Monthly means currents in February for layers 4, 7 and 10 in pressure Sigma Coordinate.

The anticyclonic eddy over the deep water of SCB extended from surface to subsurface until the fifth layer. Near the western and eastern coasts of the SCB, the southwest ward surface current varies clockwise by increasing the depth and flowing to the northeast ward on the sixth layer of sigma.

As shown in Fig. 6, the currents in the layer near the sea bottom (layer 10) are converged together into deep regions of the MCB and SCB. The divergences in the surface Ekman layer are balanced by the convergences in the bottom Ekman layer. The divergence and convergence of currents of the SCB are more stable in terms of location and intensity against than the divergence and convergence of the MCB, which is the result of the SCB's steeper bed slope.

4. Conclusion

The study aims at reproducing mean values of wind-driven currents of the CS. Monthly mean values of current speed are more important for predicting the transport of pollution compared to currents occurring at extreme storm conditions. A 3-dimensional primitive equation model is presented to simulate monthly variability of the CS circulation. Due to the vast and shallow coastal waters and deep interior regions, a numerical model with convenient vertical coordinate systems is required to simulation wind driven current in the CS. In this study, this is accomplished by using a sigma-pressure Coordinate system. This simulation reveals fundamental features of the CS circulation as upwelling along the eastern coast and an anticyclonic eddy in both SCB and MCB.

The surface current must be theoretically aligned 45° clockwise from the wind direction in the northern hemisphere, while the angle between the directions of surface current and wind is very small in the shallow water areas of the CS due to the large effects of bottom friction. In these areas the circulation pattern is very sensitive to the wind direction and speed. In the CS deep waters the direction of the surface currents are changing continuously by the Coriolis force, and establish a number of eddies in the MCB and SCB. The anticyclonic eddy is the permanent feature of the SCB and is more stable against to the circulation patterns in the NCB and MCB, as a result of more depth and steeper bed slop of the SCB. This feature is in agreement with Peeters et al. [30], who explained enhanced the vertical stability of the SCB, according to the buoyancy frequency.

The simulation of circulation pattern in the CS demonstrates that a divergence in the surface Ekman layer is balanced by a convergence in the frictional Ekman layer near the sea bottom in both the SCB and MCB. These effects show the bottom topographic features have an important role in steering currents in the CS, as also has been noted by Ghaffari et al. [31].

Comparison of the results of this simulation with the previous numerical studies shows that this model is capable to simulation circulation pattern in a basin with complex bottom topography and spatio-temporal variable wind. Also, by increasing the resolution of the depth and wind data can be more accurately simulate wind-driven currents in the CS.

5. Acknowledgments

The numerical simulations were performed under the Numerical Modeling and high performance computing laboratory at the department of Marine Physics, Tarbiat Modares University, Iran. This research is funded by "Development of a three-dimensional numerical hydrodynamic oceanic model for Caspian Sea" project.

6. References

1- Watanabe, I., Kunito, T., Tanabe, S., Amano, M., Koyama, Y., Miyazaki, N., Petrov, E. and

Tatsukawa, R., (2002), *Accumulation of heavy metals in Caspian seals (Phoca caspica)*, Archives of Environmental Contamination and Toxicology, vol.43, p.109-120.

2- Mora, S., (2006), *An assessment of marine pollution in the Caspian Sea based on the CEP 2005 contaminant survey*, Caspian Environmental Programme.Akhverdiev, I. and Demin, Y., (1989), *O structure sinopticheskih techeniy Kaspiiskogo morya v letniy sezon po rezultatam diagnosticheskih raschetov. Kaspiiskoe more. Struktura i dinamika vod*, edited by: Kosarev, AN, Nauka, Moscow, USSR, 5-15.

3- Kosarev, A.N. and Yablonskaya, E., (1994), *The Caspian Sea*, SPB Academic Publishing The Hague.

4- Ibrayev, R., Özsoy, E., Schrum, C. and Sur, H., (2010), *Seasonal variability of the Caspian Sea three-dimensional circulation, sea level and air-sea interaction*, Ocean Science Discussions 6, p.1913–1970.

5- Kara, A., Wallcraft, A.J., Joseph Metzger, E. and Gunduz, M., (2010), *Impacts of freshwater on the seasonal variations of surface salinity and circulation in the Caspian Sea*, Continental Shelf Research vol. 30, p.1211-1225.

6- Terziev, F., Kosarev, A. and Kerimov, A., (1992), *Hydrometeorology and Hydrochemistry of the USSR Seas, V6, The Caspian Sea, Issue 1 Hydrometeorological Conditions*, Gidrometeoizdat, St. Petersburg.

7- Trukhchev, D., Kosarev, A., Ivanova, D. and Tuzhilkin, V., (1995), *Numerical analysis of the general circulation in the Caspian Sea*, Dokladi na Bulgarskata Akademia na Naukite, vol. 48, p.31-34.

8- Ibrayev, R., (2001), *Model of enclosed and semi-enclosed sea hydrodynamics*, Russian Journal of Numerical Analysis and Mathematical Modelling, vol. 16, p.291-304.

9- Katunin, D. and Sapozhnikov, V., (1997), *Complex Studies of the Southern Caspian Ecosystem (Seasonal Surveys at the Research Vessel Gilyan of the Russian-Iranian Expedition, August–September 1994–February 1996)*, Okeanologiya, vol. 37, p.152-154.

10- Tuzhilkin, V., Kosarev, A., Trukhchev, D. and Ivanova, D., (1997), *Seasonal features of general circulation in the Caspian deep water part*, Meteorology and Hydrology, vol. 1, p.91-99.

11- Badalov, A. and Rzheplinski, D., (1989), *Modelirovanie dinamiki deyatelnogo sloya Kaspiiskogo morya pod deystviem sinopticheskih atmosfernyh prosessov. Modelirovanie gidrofizicheskih prosessov i poley v zamknutyh vodoemah i moryah*, Nauka, Moscow, edited by: Sarkisyan, AS, USSR, 31-51

12- Sarkisyan, A., Zaripov, B., Kosarev, A. and Rzheplinski, D., (1976), *Diagnosticheskie raschety techeniy v Kaspiiskom more*, Izvestiya RAN, Atmospheric and Oceanic Physics, vol. 12, p.1106-1110.

13- Akhverdiev, I. and Demin, Y., (1989), *O structure sinopticheskih techeniy Kaspiiskogo morya v letniy sezon po rezultatam diagnosticheskih raschetov. Kaspiiskoe more. Struktura i dinamika vod*, edited by: Kosarev, AN, Nauka, Moscow, USSR, 5-15.

14- Korotenko, K., Mamedov, R., Kontar, A. and Korotenko, L., (2004), *Particle tracking method in the approach for prediction of oil slick transport in the sea: modelling oil pollution resulting from river input*, Journal of Marine Systems, vol. 48, p.159-170.

15- Kara, A., Wallcraft, A.J., Joseph Metzger, E. and Gunduz, M., (2010), *Impacts of freshwater on the seasonal variations of surface salinity and circulation in the Caspian Sea*, Continental Shelf Research vol. 30, p.1211-1225.

16- Gunduz, M. and Özsoy, E., (2013), *Modelling Seasonal Circulation and Thermohaline Structure of the Caspian Sea*, Ocean Science Discussions, 11. 10.5194/osd-11-259-2014.

17- Ibrayev, R., Sarkisyan, A. and Trukhchev, D., (2001), *Seasonal variability of circulation in the Caspian Sea reconstructed from normal hydrological data*, Izvestiia RAN, Atmospheric and Oceanic Physics, vol. 37, p.96-104.

18- Zounemat Kermani, M. and Sabbagh Yazdi, S.R., (2010), *Conjunction of 2D and 3D modified flow solvers for simulating spatio-temporal wind induced hydrodynamics in the Caspian Sea*, Ocean Science, vol. 45, p.113-128.

19- Kitazawa, D. and Yang, J., (2012), *Numerical analysis of water circulation and thermohaline structures in the Caspian Sea*, Journal of marine science and technology, vol. 17, p.168-180.

20- Nasimi, S. and Ghiassi, R., (2006), *A three-dimensional model of water circulation and temperature structure in the Caspian Sea*. Environmental Problems in Coastal Regions VI: p.261-272.

21- Phillips, N.A., (1957), *A coordinate system having some special advantages for numerical forecasting*, Journal of Meteorology, vol. 14, p.184-185.

22- Kasahara, A., (1974), *Various vertical coordinate systems used for numerical weather prediction*, Monthly Weather Review, vol. 102, p.509-522.

23- Gill, A.E., (2016), *Atmosphere and Ocean Dynamics*, Academic Press, New York.

24- Haltiner, G.J.W. and Williams, R., (1980), *Numerical prediction and dynamic meteorology*, 2nd Edition, Wiley, New York, 496 p.

25- Wu, J., (1982), *Wind-stress coefficients over sea surface from breeze to hurricane*, Journal of Geophysical Research, vol. 87, p.9704-9706.

26- Nihoul, J.C., (1977), *Three-dimensional model of tides and storm surges in a shallow well-mixed continental sea*, Dynamics of Atmospheres and Oceans, vol. 2, p.29-47.

27- Li, Y. and Zhan, J., (1993), *An efficient three-dimensional semi-implicit finite element scheme for simulation of free surface flows*, International journal for numerical methods in fluids, vol. 16, p.187-198.

28- Ibraev, I., Ozsoy, E., Ametistova, L., Sarkisyan, A. and Sur, H., (1998), *Seasonal variability of the Caspian Sea dynamics: barotropic motion driven by climatic wind stress and Volga River discharge*, In: Konstantin Fedorov Memorial Symposium, Sankt-Petersburg, Pushkin, St. Petersburg, p.18-22.

29- Lednev, V., (1943), *Techeniya Severnogo i Srednego Kaspiya*. Morskoy Transport, Moscow, USSR.

30- Peeters, F., Kipfer, R., Achermann, D., Hofer, M., Aeschbach-Hertig, W., Beyerle, U., Imboden, D.M., Rozanski, K. and Fröhlich, K., (2000), *Analysis of deep-water exchange in the Caspian Sea based on environmental tracers*, Deep Sea Research Part I: Oceanographic Research Papers, vol. 47, p.621-654.

31- Ghaffari, P., Isachsen, P. and LaCasce, J., (2013), *Topographic effects on current variability in the Caspian Sea*, Journal of Geophysical Research, Oceans 118, p.7107-7116.